Interlayer Interactions in Low-Dimensional Layered Hetero-Structures: Modeling and Applications

Oded Hod

Contents

Abstract

The field of nanoscale material science has experienced a true revolution over the past 30 years with the discovery of the quasi-zero- and one-dimensional cage-like structures of fullerenes and nanotubes. The successful isolation of graphene about a century ago has further triggered an avalanche of studies unraveling its unique physical and chemical properties. This, in turn, has led to numerous breakthroughs of basic science nature as well as diverse potential technological applications in the fields of nanoscale electronics, flexible displays, solar cells, DNA sequencing, chemical sensing, composite materials, solid lubrication, and many others.

Following extensive studies of the properties of graphene, much attention was recently paid to other members of the two-dimensional (2D) hexagonal layered materials family including hexagonal boron nitride (*h*-BN) and several transition metal dichalcogenides. Interestingly, stacking individual layers of these materials to form homogeneous and heterogeneous structures results in unique

O. Hod (✉)
Department of Physical Chemistry, School of Chemistry, The Raymond and Beverly Sackler Faculty of Exact Sciences and The Sackler Center for Computational Molecular and Materials Science, Tel Aviv University, Tel Aviv, Israel
e-mail: odedhod@tau.ac.il

© Springer International Publishing AG, part of Springer Nature 2018

W. Andreoni, S. Yip (eds.), *Handbook of Materials Modeling*,
https://doi.org/10.1007/978-3-319-50257-1_38-1

physical characteristics that depend on the specific chemical composition of the system and can be tuned via the application of external perturbations. This opens numerous opportunities for combinatorial materials design with versatile structure-function relations. Understanding what determines the properties of such complex structures and how to control them remains a challenge yet to be met in order for these materials to fulfill their full potential.

Theory and computation may offer a valuable microscopic perspective toward achieving this goal. The reduced-dimensions of materials at the nanoscale allow for a unique interplay between theory, computation, and experiment. Here, accurate fully atomistic simulations can complement experiments both in analyzing and rationalizing experimental results and in providing reliable predictions that can minimize the need for demanding trial and error experimental efforts.

Such theoretical treatments of 2D materials require special attention to their anisotropic nature characterized by a strong in-plane covalent bonding network and weaker interlayer interactions. While state-of-the-art quantum mechanical approaches can simultaneously describe these interactions with high accuracy, their computational demand often limits their applicability to relatively small systems. An efficient alternative can be provided by carefully tailored classical force-fields. When appropriately parameterized against experimental results or high accuracy calculations of small model systems, these can provide a reliable description of the structural, mechanical, tribological, and heat transport properties of realistic nanoscale systems with atomic scale resolution. Such force-fields that provide a proper description of intralayer interactions in a variety of 2D materials have been developed over the years and are accessible via standard molecular dynamics simulation codes. Surprisingly, despite the great scientific interest in 2D layered materials, complementary interlayer force-fields that can accurately capture both their binding and sliding energy landscapes are currently available for a very limited set of systems.

In the present chapter, I provide a brief review of recent developments of reliable, efficient, and transferable anisotropic interlayer force-fields for homogeneous and heterogeneous low-dimensional hexagonal layered materials. To demonstrate the performance of these methods, a few applications to the study of the structural and tribological properties of quasi-one- and quasi-two dimensional layered structures will be presented.

1 Introduction

The successful isolation of graphene, a one atom thick hexagonal carbon layer, by Novoselov and Geim in 2004 marked the opening of a new era in materials science (Novoselov et al. 2004; Geim and Novoselov 2007; Li and Kaner 2008; Geim 2009; Rao et al. 2009). The study of its unique physical properties including exceptional mechanical strength (Lee et al. 2008), superlubric tribological characteristics (Dienwiebel et al. 2004; Koren et al. 2015), remarkable room temperature electron mobilities (Novoselov et al. 2005a; Morozov et al. 2008), high thermal

conductivity (Balandin et al. 2008; Cai et al. 2010; Xu et al. 2014), quasi-relativistic electronic structure (Geim and Novoselov 2007), and controllable optical properties is flourishing even more than a decade later. Nevertheless, despite this wealth of outstanding material characteristics, the semi-metallic nature of graphene limits its applicability in switchable nanoscale electronic devices. This has triggered the scientific community to search for graphene alternatives within the diverse family of layered inorganic materials (Novoselov et al. 2005b, 2016; Deng et al. 2016).

Currently, two-dimensional (2D) inorganic materials are at the forefront of scientific research with an ever-growing number of chemical compositions including hexagonal boron nitride (*h*-BN), germanene, silicene, phosphorene, transition metal dichalcogenides, such as molybdenum and tungsten disulfide (*2H*-MoS_2 and *2H*-WS_2) and diselenide (*2H*-$MoSe_2$ and *2H*-WSe_2), among others (Heine 2015; Li and Zhu 2015). Similar to graphene, these materials exhibit diverse physical properties and appear in many structural forms ranging from planar configurations to nanotubes, scrolls, onions, and cones.

The recently demonstrated ability to stack such 2D materials in homogeneous as well as heterogeneous few-layered structures (Novoselov et al. 2016; Deng et al. 2016; Dean et al. 2010; Geim and Grigorieva 2013; Wang et al. 2014; Das et al. 2015) opens a vast combinatorial material space enabling the design of novel structures exhibiting desired physical properties. Furthermore, electromechanical manipulation of such structures can be used to gain control over their physical properties – a basic requirement for their future technological application (Koren et al. 2015, 2016; Leven et al. 2013).

Here, theory and computation play a prominent role in efficiently scanning the vast material space, identifying potential candidates that are expected to exhibit the desired physical properties, and studying their sensitivity towards external perturbations. This can focus the demanding experimental efforts on a selected group of predesigned structures and increase the probability of obtaining the required 2D material functionality. Moreover, a synergic cooperation between theory, computation, and experiment, where experimental data are used to refine theoretical models and computational algorithms that, in turn, provide more accurate predictions, can formulate a feedback cycle that will considerably enhance the efficiency of 2D materials design.

An accurate theoretical account of the physical and chemical properties of layered (and other) materials requires a full quantum mechanical treatment of their electronic structure. Computational methodologies that may provide such ultimate accuracy include wave function-based configuration interaction or coupled clusters methods as well as quantum Monte-Carlo procedures (Nightingale and Umrigar 1999; Pang 2016). These methods, however, are quite unfavorable in terms of the scalability of their computational burden with system size and are hence limited to very small molecular structures. Green's function-based methods that can efficiently sum high-order terms in a perturbative expansion scale better with system size and hence can treat somewhat larger systems (Sakai et al. 2015). Density functional theory (DFT) (Hohenberg and Kohn 1964; Kohn and Sham 1965) is currently probably the most popular method to study the physical properties of large systems

(Sakai et al. 2015). While being exact in principle, its practical approximations provide a good balance between computational efficiency and accuracy. Nowadays, DFT calculations of material properties involving hundreds of atoms are being routinely performed in many research groups (Barone et al. 2011). If one desires to treat even larger systems on a fully atomistic and quantum mechanical basis, accuracy is often further compromised to gain computational efficiency. Here, methods like the variational Hartree-Fock formalism (Szabo and Ostlund 1989), semi-empirical approaches (Pople 1970), density functional based tight-binding approximations (Porezag et al. 1995; Kwon and Tománek 2000; Miró et al. 2013; Zahid et al. 2013), or empirical tight-binding (Szabados et al. 2006; Carlson and Dumitrică 2007) can be used to provide approximate descriptions of 2D material properties.

Often, however, a fully quantum mechanical treatment is not required and a much simplified classical picture is sufficient to efficiently and accurately describe many material properties. Specifically, when considering static structural and mechanical properties of various materials (Chen et al. 2013; Butz et al. 2014; van Wijk et al. 2015) as well as their dynamic tribological (Guo et al. 2007; Guerra et al. 2010; Reguzzoni et al. 2012a; Vanossi et al. 2013; van Wijk et al. 2013; Xu et al. 2013; Ze 2014; Kang and Lee 2014) and heat transport characteristics (Jiang 2014a), Newtonian dynamics with carefully designed force-fields (FF) can provide valuable insights (Frenkel and Smit 2002; Allen and Tildesley 2009; Rapaport 2009). Obviously, this results in considerable computational gain enabling the treatment of extremely large atomistic models including tens of thousands of atoms for relatively long timescales. Furthermore, it allows for devising multiscale approaches, where the information gained from fully atomistic calculations serves to design coarse-grained and continuum models. Nevertheless, this comes at the expense of neglecting explicit quantum mechanical effects and even more importantly the need to design system specific interatomic potentials with limited transferability.

With this respect, the formulation of dedicated force-fields for 2D materials and their layered constructs has to account for their inherent structural anisotropy. The individual layers can be viewed as a network of covalently bonded atoms organized in a periodic hexagonal lattice structure. Upon stacking, each layer interacts with its neighboring counterparts via long-range dispersion and electrostatic interactions. Hence, a strategy involving a separate treatment of intralayer and interlayer interactions is often invoked.

2 Intralayer Interactions

The intralayer force-field term usually involves six main ingredients including (see Fig. 1): (http://cbio.bmt.tue.nl/pumma/index.php/Theory/Potentials; Rappe et al. 1992) (i) bonded two-body interactions describing the bond stretching and compression energy; (ii) bonded three-body interactions accounting for angle bending penalties; bonded four-body interactions depicting (iii) improper and (iv) dihedral

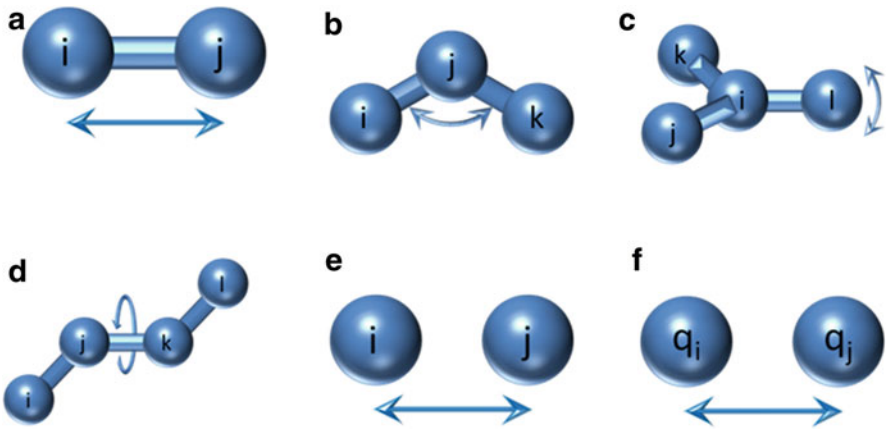

Fig. 1 Illustration of several intralayer force-field term contributions: (**a**) Bond stretching and compression; (**b**) angle bending; (**c**) improper angle deformation; (**d**) torsional angle deformation; (**e**) van der Waals interactions; (**f**) electrostatic interactions

torsional deformations; (v) nonbonded van der Waals (vdW) interactions; and (vi) nonbonded electrostatic interactions.

The first two components are often represented by simple harmonic springs of the form $V_{ij}^{(\mathrm{i})}\left(r_{ij}\right) = k_{ij}\left(r_{ij} - r_{ij}^{0}\right)^{2}$ and $V_{ijk}^{(\mathrm{ii})}\left(\theta_{ijk}\right) = k_{ijk}\left[\cos\left(\theta_{ijk}\right) - \cos\left(\theta_{ijk}^{0}\right)\right]^{2}$. Here, r_{ij} is the distance between atomic center i and j, θ_{ijk} is the angle defined by atomic centers i, j and k (see Fig. 1a, b), r_{ij}^{0} and θ_{ijk}^{0} are the equilibrium ij pair interatomic distance and ijk triad angle, respectively, and k_{ij} and k_{ijk} are the corresponding force constants. Improper torsion is often also described by a harmonic potential of the form $V_{ijkl}^{(\mathrm{iii})}\left(\delta_{ijkl}\right) = k_{ijkl}^{(\mathrm{iii})}\left(\delta_{ijkl} - \delta_{ijkl}^{0}\right)^{2}$, δ_{ijkl} being the improper angle (see Fig. 1c) and $k_{ijkl}^{(\mathrm{iii})}$ and δ_{ijkl}^{0} being the corresponding force constant and equilibrium improper angle, respectively. Dihedral angle torsion can be depicted by a periodic potential of the form $V_{ijkl}^{(\mathrm{iv})}\left(\phi_{ijkl}\right) = k_{ijkl}^{(\mathrm{iv})}\left[1 + \cos\left(\eta_{ijkl}\phi_{ijkl} - \phi_{ijkl}^{0}\right)\right]$, where ϕ_{ijkl} is the dihedral angle (see Fig. 1d), $k_{ijkl}^{(\mathrm{iv})}$ is the corresponding force constant, ϕ_{ijkl}^{0} sets the equilibrium dihedral angle, and η_{ijkl} is the multiplicity factor signifying the number of minima that this potential term possesses. The nonbonded vdW term is often described by the two-body Lennard-Jones (LJ) potential of the form $V_{ij}^{(\mathrm{v})}\left(r_{ij}\right) = 4\epsilon_{ij}\left[\left(\sigma_{ij}/r_{ij}\right)^{12} - \left(\sigma_{ij}/r_{ij}\right)^{6}\right]$ where ϵ_{ij} and $\sqrt[6]{2}\sigma_{ij}$ are the binding energy and equilibrium distance of the ij atomic pair, respectively (see Fig. 1e). Note that this expression accounts not only for the long-range attractive vdW interactions but also for short-range repulsions. Finally, interatomic monopolar electrostatic interactions are calculated using Coulombs law $V_{ij}^{(\mathrm{vi})}\left(r_{ij}\right) = q_i q_j / \left(4\pi\epsilon_0 r_{ij}\right)$, where ϵ_0 is the vacuum permittivity and q_k is the effective partial charge of atom k (see Fig. 1f).

It should be noted that while the expressions described above are commonly used to describe the intralayer interactions in layered materials they are, by no means, the only ones available. For example, if a reactive force-field is required, the harmonic bonded two-body terms can be replaced by an anharmonic potential that allows for bond breaking and formation. Furthermore, the force-field parameters can be varied according to the local chemical environment, thus providing flexibility to describe different bond-orders and accounting for various chemical binding schemes.

The various force-field parameters have to be determined separately for each material. The fitting procedure can be performed against experimentally measured material properties, such as the Young modulus, the shear modulus, lattice constants, phonon spectra, and heats of formation. Alternatively, they can be calibrated to fit results of higher accuracy methods such as state-of-the-art DFT calculations. Dedicated intralayer force-field parameterizations are available for a variety of layered materials including graphene and its derivatives (Al-Jishi and Dresselhaus 1982; Tersoff 1988; Brenner 1988, 1990; Stuart et al. 2000; Brenner et al. 2002; Los and Fasolino 2003; Ghiringhelli et al. 2005a, 2008; Los et al. 2005; Perebeinos and Tersoff 2009; Lindsay and Broido 2010; Jiang 2015; O'Connor et al. 2015), *h*-BN (Sevik et al. 2011), and *2H*-MoS_2 (Jiang 2015; Wakabayashi et al. 1975; Jiménez Sandoval et al. 1991; Brunier et al. 1992; Morita et al. 2008; Liang et al. 2009; Varshney et al. 2010; Jiang et al. 2013; Nicolini and Polcar 2016), many of which are implemented in open source or commercial software packages. These have been successfully used to describe a variety of material properties including the structural and mechanical behavior (Tersoff 1992; Lu 1997; Hertel et al. 1998; Fasolino et al. 2007; Bets and Yakobson 2009; Costamagna et al. 2012; Singh et al. 2013, 2015; Bucholz and Sinnott 2013; Jin-Wu et al. 2013; Jiang 2014b; Jiang and Park 2014), thermal transport characteristics (Varshney et al. 2010; Che et al. 2000; Mohamed and Deepak 2001; González Noya et al. 2004; Yao et al. 2005; Lindsay and Broido 2011), crack propagation (Xiaonan et al. 2015), and melting dynamics of 2D monolayers (Singh et al. 2015).

3 Interlayer Interactions

The interlayer force-field term usually involves three main contributions: long-range attractive vdW interactions, short-range Pauli repulsions, and electrostatic interactions. The latter, which is required when atoms in different layers have a sizable partial charge, can often be described by a simple Coulombic term similar to the $V_{ij}^{(\mathrm{vi})}$ intralayer expression given above (see Fig. 1f). To describe the attractive vdW and repulsive Pauli interactions, the LJ (or Morse (Los and Fasolino 2003; Los et al. 2005; Ghiringhelli et al. 2005b; Karssemeijer and Fasolino 2011)) potential is often chosen similar to the intralayer $V_{ij}^{(\mathrm{v})}$ expression (see Fig. 1e) (Nicolini and Polcar 2016; Lebedeva et al. 2011a; Shibuta and Elliott 2011; Ye et al. 2012, 2015; Jayasena et al. 2013; Liu et al. 2015; Kushima et al. 2015). With appropriate parameterization, this expression can provide a good description of the interlayer

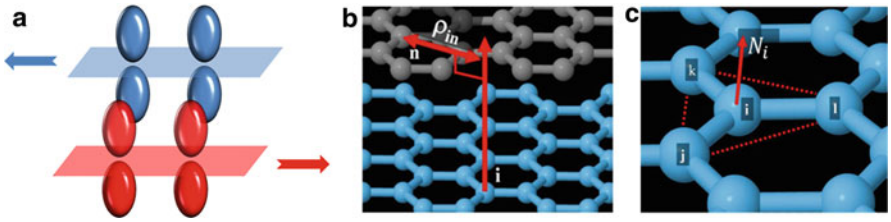

Fig. 2 Anisotropic Pauli repulsion term: (**a**) illustration of the anisotropic p_z orbital overlap variations during interlayer sliding; (**b**) definition of the lateral interatomic distance; (**c**) definition of the local surface normal. (Reprinted with permission from Oz et al. (2016). Copyright (2016) American Chemical Society)

binding energy curve (Szabados et al. 2006; Jiang 2015; Brunier et al. 1992; Varshney et al. 2010; Jiang et al. 2013; Lu 1997; Bucholz and Sinnott 2013; Jiang and Park 2014; Singh et al. 2015; Girifalco and Lad 1956; Green et al. 1974; Weiss and Phillips 1976; Kuzuba et al. 1985; Lu et al. 1992; Tersoff and Ruoff 1994; Kwon and Tománek 1998; Buldum and Lu 1999; Girifalco et al. 2000; Girifalco and Hodak 2002; Qian et al. 2003; Michel and Verberck 2011; Tolga et al. 2016). However, using the same parameters to study relative interlayer sliding fails to reproduce the corrugated sliding energy landscape and results in too shallow energy barriers (Carlson and Dumitrică 2007; Stuart et al. 2000; Palser 1999; Kolmogorov and Crespi 2000, 2005; Shtogun and Woods 2010; Lebedeva et al. 2011b; Reguzzoni et al. 2012b; Neek-Amal and Peeters 2014; Strutyński et al. 2014; Korhonen and Koskinen 2015; Jiang and Park 2015). Hence, the ability of LJ type potentials to reliably describe many structural, mechanical, and tribological properties of layered materials may be considerably hindered.

The origin of this deficiency in the LJ potential was identified by Kolmogorov and Crespi (KC) to be the use of isotropic expressions that depend only on interatomic distances to describe an anisotropic material property (Kolmogorov and Crespi 2000, 2005; Lebedeva et al. 2011b). Focusing on graphene, KC realized that when two layers slide upon each other, electron clouds associated with the p_z orbitals around carbon atoms residing on adjacent layers overlap as the atoms pass each other (see Fig. 2a). This, in turn, induces Pauli repulsion variations resulting in a corrugated sliding energy landscape. Since the electron density overlap depends on the lateral distance between the crossing atoms, an interlayer pair-potential of the following form was suggested (Kolmogorov and Crespi 2005):

$$V^{\mathrm{KC}}(r_{in}, \rho_{in}) = e^{-\lambda(r_{in}-z_0)}\left[C + f(\rho_{in}) + f(\rho_{ni})\right] - A(r_{in}/z_0)^{-6}. \tag{1}$$

This expression includes a LJ type long-range attractive term scaled by $A = 10.238$; an isotropic Morse-like short-range exponential repulsive term with the equilibrium interlayer distance $z_0 = 3.34$ Å, exponent $\lambda = 3.629$ Å^{-1}, and scaling factor $C = 3.030$; and an anisotropic short-range Gaussian repulsive term

of the form $f(\rho) = e^{-(\rho/\delta)^2} \Sigma_n c_{2n} (\rho/\delta)^{2n}$ that depends on the lateral distance, ρ, between each pair of atoms on adjacent layers scaled by $\delta = 0.578$ Å. The nonzero coefficients of the polynomial multiplying the Gaussian are given by $c_0 = 15.71$, $c_2 = 12.29$, and $c_4 = 4.933$. The lateral distance, ρ_{in}, is defined as the shortest distance between atom n on one layer and the surface normal at atom i residing on an adjacent layer (see Fig. 2b). For a hexagonal lattice, the simplest definition of the local surface normal at a given atomic position is the unit vector perpendicular to the triangle formed by its three nearest neighbors (see Fig. 2c). Since for curved systems generally $\rho_{in} \neq \rho_{ni}$ the pair potential is symmetrized to fulfill Newton's third law. With the inclusion of the anisotropic repulsive term, the KC potential was shown to simultaneously provide a good description of both interlayer binding and sliding energy landscapes (see Fig. 3) (Kolmogorov and Crespi 2000, 2005; Reguzzoni et al. 2012b).

Despite this notable success and the ever growing interest in 2D materials, the KC approach (and related methods (Lebedeva et al. 2011b, 2012; Popov et al. 2011)) has not been extended to describe other layered materials for more than a decade since its inception. Recently, however, the transferability of the method was demonstrated where a KC type potential was applied to the graphene/*h*-BN hetero-structure (van Wijk et al. 2014; Woods et al. 2016). In this study, the FF parameters have been set to reproduce experimentally observed moiré superstructures arising from the 1.8% intralayer lattice constant mismatch between graphene and *h*-BN. This indicated the ability of the KC force-field to describe the structural properties of homogeneous and heterogeneous junctions of 2D materials.

To harness the full predictive capabilities of KC-type FFs to describe the interlayer interactions in a variety homogeneous and heterogeneous layered materials structures, a slightly modified functional form, termed interlayer potential (ILP), was recently suggested. The ILP accounts for monopolar electrostatic interactions and allows for simple parameterization against state-of-the-art first-principles calculations based on pair-wise (Tkatchenko and Scheffler 2009; Marom et al. 2011) and many-body dispersion corrected (Tkatchenko et al. 2012; Ambrosetti et al. 2014) screened-hybrid (Heyd et al. 2003; Heyd and Scuseria 2004a, b) density functional theory calculations (Leven et al. 2014, 2016a; Maaravi et al. 2017; https://pubs.acs.org/doi/10.1021/acs.nanolett.8b02848).

The ILP consists of a modified KC **short-range anisotropic repulsive term** of the form:

$$V_{Rep}(r_{in}, \rho_{in}) = \mathrm{Tap}(r_{in}) \times e^{\alpha_{in}\left(1-\frac{r_{in}}{\beta_{in}}\right)} \left[\varepsilon_{in} + C_{in}\left(e^{-\left(\frac{\rho_{in}}{\gamma_{in}}\right)^2} + e^{-\left(\frac{\rho_{ni}}{\gamma_{in}}\right)^2}\right)\right], \qquad (2)$$

where ε_{in} and C_{in} are constants setting the energy scales associated with the isotropic and anisotropic repulsion, respectively, β_{in} and γ_{in} set the corresponding interaction ranges, and α_{in} is a parameter defined to set the steepness of the isotropic repulsion term. Note that for computational efficiency, the 4th degree polynomial multiplying the anisotropic Gaussian

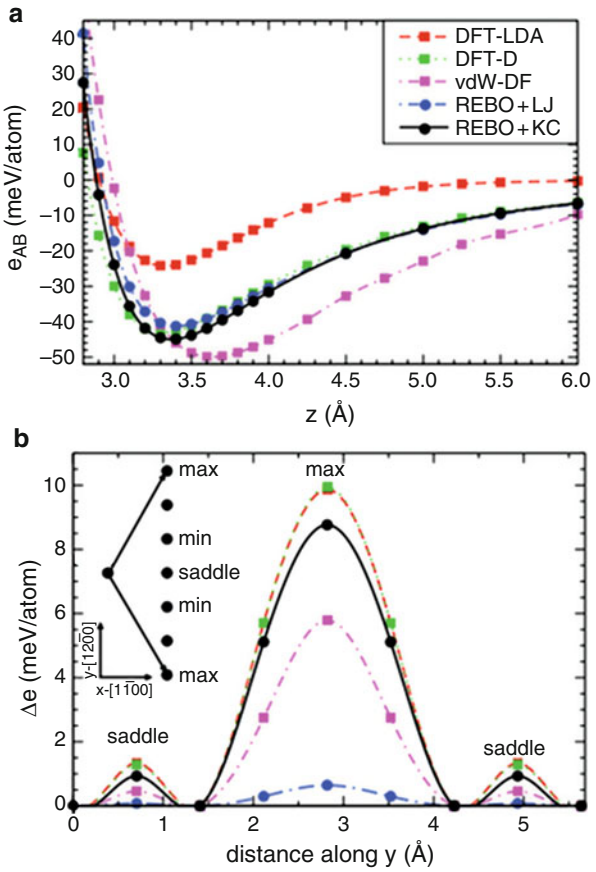

Fig. 3 Interlayer (**a**) binding and (**b**) sliding energy curves of bilayer graphene calculated using the LJ (full blue circles) and KC (full black circles) interlayer potentials compared to a reference dispersion corrected DFT calculation (full green squares). (Reprinted with permission from Reguzzoni et al. (2012b). Copyright (2012) by the American Physical Society)

repulsion term appearing in the original KC expression (see Eq. (1) above) is replaced by a constant factor. Furthermore, a taper function of the form $\mathrm{Tap}(r_{in}) = 20(r_{in}/R_{cut})^7 - 70(r_{in}/R_{cut})^6 + 84(r_{in}/R_{cut})^5 - 35(r_{in}/R_{cut})^4 + 1$, which provides a continuous (up to third derivative) cutoff for interatomic separations exceeding R_{cut}, is used to damp the long-range contribution of the repulsive term. These modifications simplify the FF expressions and reduce the computational cost while providing a satisfactory description of the interlayer interactions (Leven et al. 2014, 2016a; Maaravi et al. 2017).

To treat the **long-range attractive interactions,** the Tkatchenko and Scheffler (TS) dispersion correction scheme to DFT is considered (Tkatchenko and Scheffler 2009). Within this approach, widely used semi-local or hybrid exchange-correlation

density functional approximations that are known to provide an inadequate description of long-range van der Waals (vdW) interactions are augmented by a term that decays asymptotically with the interatomic distance as r^{-6}. This term is damped at short distances to avoid double-counting of short-range correlation effects. In the ILP, the following pair-wise long-range attractive term is adopted:

$$V_{Att}\left(r_{in}\right) = \mathrm{Tap}\left(r_{in}\right)\left\{-\left[1+e^{-d\left[\left(r_{in}/\left(S_R\cdot r_{in}^{eff}\right)\right)-1\right]}\right]^{-1}\cdot\frac{C_{6,in}}{r_{in}^{6}}\right\}. \tag{3}$$

Here, r_{in}^{eff} is the sum of effective equilibrium vdW atomic radii of atom i and atom n residing on different layers, $C_{6,\,\mathrm{in}}$ is the pair-wise dispersion coefficient of the two atoms in the solid-state environment, and d and S_R are unit-less parameters defining the steepness and onset of the short-range Fermi-Dirac type damping function. Similar to the repulsive term, long-range taper damping is implemented to reduce computational burden. This specific form is chosen as it allows the extraction of the various parameters directly from first-principles calculations avoiding the need for experimental data that is macroscopic by nature, very difficult to obtain, and mostly unavailable for many 2D layered materials and hetero-structures thereof.

In cases where atoms residing on the interacting layers bear sizable effective charges, electrostatic contributions should be taken into account. To this end, the formalism implemented in the ReaxFF scheme can be utilized (van Duin et al. 2001). Within this approach, a shielded Coulomb potential term of the form:

$$V_{Coul}\left(r_{in}\right) = \mathrm{Tap}\left(r_{in}\right)\times\left[kq_iq_n/\sqrt[3]{r_{in}^{3}+\left(1/\lambda_{in}\right)^{3}}\right] \tag{4}$$

is used. Here, k is Coulomb's constant and λ_{in} is a shielding parameter introduced to eliminate the short-range singularity of the classical monopolar electrostatic interaction expression. This shielding takes effect in regions where Pauli repulsions between overlapping electron clouds dominate the interlayer potential and hence has minor influence on the results. When considering periodic systems, the long-range taper cutoff can be replaced by Ewald summation techniques (Ewald 1921; Toukmaji and Board 1996) in order to avoid conditionally convergent sums (Hod 2012a).

In many cases, the effective ionic charges, q_i and q_n, can be treated as constant values throughout the simulation. Nevertheless, in order to provide a general description, they can be dynamically evaluated using the electronegativity equalization method (EEM) (van Duin et al. 2001; Mortier et al. 1986; Njo et al. 1998; Bultinck et al. 2002). This method relies on a principle formulated by Sanderson stating that when a molecule or a solid is formed, the electronegativities of the constituent atoms equalize to give a global electronegativity of the entire system (Sanderson 1951, 1983). Hence, the electronegativity of a given atom within the molecular or solid environment (χ_i) is written in terms of the corresponding

isolated atom electronegativity (Parr et al. 1978) $\left(\chi_i^0\right)$ and hardness (Parr and Pearson 1983; Sanderson 1976) $\left(\eta_i^0\right)$ as $\chi_i = \left(\chi_i^0 + \Delta\chi_i\right) + 2\left(\eta_i^0 + \Delta\eta_i\right)q_i + \sum_{j\neq i} kq_j/\sqrt[3]{r_{ij}^3 + \left(1/\lambda_{ij}\right)^3}$. Here, $\Delta\chi_i$ and $\Delta\eta_i$ represent the electronegativity and hardness variations due to the embedding molecular or solid environment and the last term represents the electrostatic potential induced by all other atoms in the system (Weismiller et al. 2010). The effective atomic charges can then be obtained by enforcing the guiding principle that within the molecular or solid environment all atomic electronegativities should equal the equilibrated molecular electronegativity $\chi_{i=1\ldots N} = \chi_{eq}$. To this end, the following matrix equation is solved:

$$\begin{pmatrix} 2\left(\eta_1^0+\Delta\eta_1\right) & k/\sqrt[3]{r_{12}^3+(1/\lambda_{12})^3} & \cdots & k/\sqrt[3]{r_{1N}^3+(1/\lambda_{1N})^3} & -1 \\ k/\sqrt[3]{r_{21}^3+(1/\lambda_{21})^3} & 2\left(\eta_2^0+\Delta\eta_2\right) & \cdots & k/\sqrt[3]{r_{2N}^3+(1/\lambda_{2N})^3} & -1 \\ \vdots & \vdots & \ddots & \vdots & \vdots \\ k/\sqrt[3]{r_{N1}^3+(1/\lambda_{N1})^3} & k/\sqrt[3]{r_{N2}^3+(1/\lambda_{N2})^3} & \cdots & 2\left(\eta_N^0+\Delta\eta_N\right) & -1 \\ 1 & 1 & \cdots & 1 & 0 \end{pmatrix} \begin{pmatrix} q_1 \\ q_2 \\ \vdots \\ q_N \\ \chi_{eq} \end{pmatrix} = -\begin{pmatrix} \chi_1^0+\Delta\chi_1 \\ \chi_2^0+\Delta\chi_2 \\ \vdots \\ \chi_N^0+\Delta\chi_N \\ -Q \end{pmatrix}, \tag{5}$$

where the isolated atomic electronegativities and hardnesses, χ_i^0 and η_i^0, their corresponding molecular or solid environment variations $\Delta\chi_i$ and $\Delta\eta_i$, and the total charge, Q, are provided as input. The latter is dictated by the modeled system, whereas the former are used as fitting parameters.

While originally parameterized for homogeneous *h*-BN and graphene junctions (Leven et al. 2014; Maaravi et al. 2017), as well as for heterogeneous junctions thereof (Leven et al. 2016a), with appropriate parameterization the ILP should be transferable to a variety of layered materials such as different graphene allotropes including pentaheptite, haeckelite, dimerite, and octite (David et al. 2010); graphane; graphyne; germanene; silicene; stanene; phosphorene; and members of the transition metal dichalcogenides family such as molybdenum and tungsten disulfide and diselenide. As demonstrated in the next section, such an extension will make the ILP a versatile and powerful simulation tool for the study of the structural, mechanical, dynamic, and heat transport properties of homogeneous and heterogeneous layered material structures.

4 Applications

An illustrative demonstration of the performance of classical ILPs for studying interlayer interactions in layered materials is the case of the graphene/*h*-BN heterojunction. This heterojunction has gained great attention from the scientific community in recent years (Geim and Grigorieva 2013; Wang et al. 2014; Das et al. 2015; Leven et al. 2016a) due to its rich physical properties that include a controllable electronic band-gap (Chen et al. 2014; Fan et al. 2011; Jung et al. 2015; Yankowitz et al. 2012), ultrahigh electron mobility (Dean et al. 2010; Levendorf et

al. 2012; Tang et al. 2013), the demonstration of Hofstadter's butterfly phenomenon (Ponomarenko et al. 2013; Dean et al. 2013), and the manifestation of controllable hyperbolic meta-material characteristics (Dai et al. 2015).

Owing to the intrinsic lattice-constant mismatch between graphene and *h*-BN, the former tends to deform when placed on a multilayer *h*-BN substrate in order to adapt to the underlying crystal lattice (van Wijk et al. 2014; Yankowitz et al. 2012; Dean et al. 2013; Yang et al. 2013; Woods et al. 2014). The resulting moiré superstructures alter graphene's electronic and optical properties thus opening new opportunities for technological applications (Jung et al. 2015; Kumar et al. 2015). Naturally, modeling such superstructures from first-principles is a prohibitively demanding task. This, in turn, calls for the utilization of classical ILPs.

Figure 4 presents the fully relaxed structure of a free-standing graphene/*h*-BN bilayer supercell calculated using the graphene/*h*-BN ILP (Leven et al. 2016a). A clear moiré superstructure is obtained (see panel (d)), where regions of optimal interlayer registry (blue regions in panel (a)) and distance (blue regions in panel (b)) and intralayer bond lengths (red regions in panel (c)) are separated by sharp domain walls characterized by increased interlayer distance and compressed intralayer bond lengths in accordance with experimental findings (Yankowitz et al. 2012; Woods et al. 2014). Furthermore, due to the lack of rigid support, the calculation predicts that the entire structure should become highly corrugated. This latter observation was recently verified experimentally (Argentero et al. 2017).

Such moiré superstructures are expected to have considerable effect on the tribological properties of the heterojunctions. To investigate this, the graphene/*h*-BN ILP (Leven et al. 2016a) has been recently used to simulate the frictional

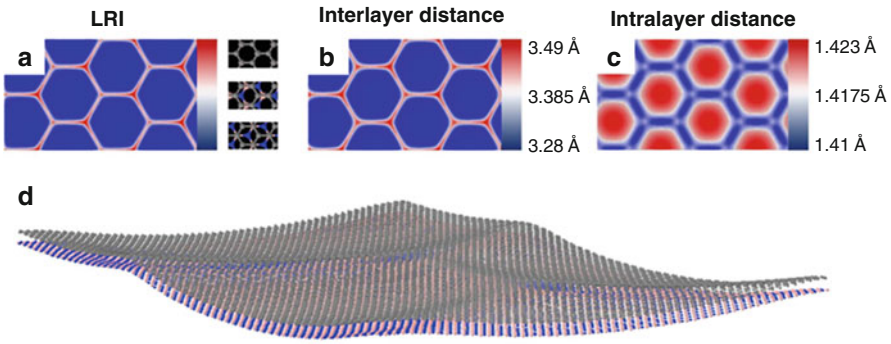

Fig. 4 Fully relaxed graphene/*h*-BN free-standing bilayer. (**a**) Local registry index map, where blue and red colors represent optimal and worst interlayer stacking, respectively. The calculation is performed using the registry index method that defines a purely geometric quantitative measure of interlattice commensurability (Leven et al. 2013, 2016a; Koren et al. 2016; Marom et al. 2010; Hod 2010, 2012b, 2013; Blumberg et al. 2012; Garel et al. 2012; Oz et al. 2016; Leven et al. 2016b); (**b**) interlayer distance map; (**c**) graphene intralayer bond-length map; and (**d**) overall structure of a fully relaxed, free-standing, graphene/*h*-BN bilayer. (Reprinted with permission from Leven et al. (2016a). Copyright (2016) American Chemical Society)

behavior of the heterojunction (Mandelli et al. 2017). It was found that for the aligned interface (where the lattice vectors of the two layers are parallel), with contact size below the characteristic lateral dimension of the elevated superstructure ridges, the junction behaves like its homogeneous counterparts with friction forces that grow linearly with the contact area. Superlubricity sets in due to the progressive appearance of moiré patterns resulting in a transition to collective stick-slip motion of the ridges that eventually turns into smooth soliton-like sliding with increasing contact size (see Fig. 5). For angularly misaligned contacts (where the lattice vectors of the two layers are rotated with respect to each other), incommensurability effects, also appearing in homogeneous junctions, are enhanced and the friction coefficients further drop by orders of magnitude and remain extremely low, even under external loads. These simulations indicated the potential of achieving robust superlubricity, independent of the relative interfacial orientation, and sustainable under external loads, in practical applications utilizing two-dimensional layered materials heterojunctions.

A similar phenomenon is found to occur in homogeneous multiwalled nanotubes, where the lattice mismatch results from the curvature difference between adjacent nanotube walls. Due to the frustrated geometry of the tube's circumference, this may result in a pronounced faceted superstructure, where the circular cross-section is deformed into a more stable polygonal one (Garel et al. 2012, 2014; Liu and Cowley 1994; Gogotsi et al. 2000; Zhang et al. 2003, 2005; Celik-Aktas et al. 2005a; Golberg et al. 2007a, b; Nigues et al. 2014). For narrow nanotubes, the excessive stain involved in the formation of sharp vertices is not compensated by the energy gain of forming the planar facets; hence, faceting is suppressed. However, above a certain nanotube diameter, typically of 12 nm (Garel et al. 2012), the standard circular cross section can be strongly distorted and faceting may appear (see Fig. 6).

Here, as well, modeling such systems from first-principles is impractical and classical ILPs serve as a viable alternative for studying their structural and mechanical properties. Hence, to decipher the mechanism that underlies facet formation and dictates their character, elaborate geometry relaxations of a wide set of double-walled carbon and boron nitride nanotubes were performed (Leven et al. 2016b). It was found that regardless of the nanotube identity (namely, diameter, and chemical composition), chiral angle matching between adjacent layers is a necessary condition for the formation of faceting. Considering first achiral nanotubes, where

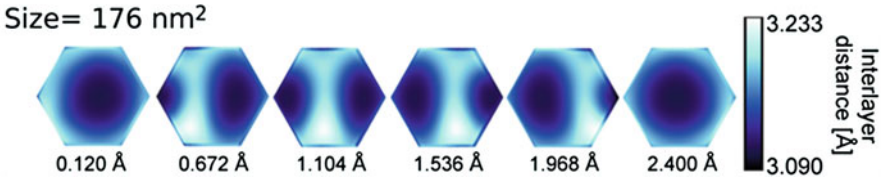

Fig. 5 Snapshots of the soliton-like smooth sliding motion of the moiré superstructure ridges occurring upon shearing of a graphene/*h*-BN junction. (Reprinted with permission from Mandelli et al. (2017). Copyright (2017) American Chemical Society)

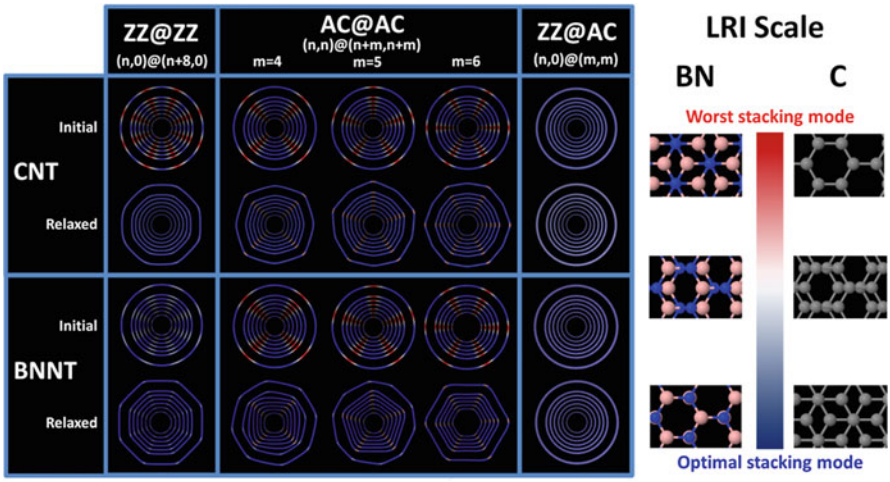

Fig. 6 Schematic representation of achiral double-walled carbon (top two rows) and boron-nitride (bottom two rows) nanotubes, showing their structure and local registry patterns prior to and after geometry relaxation. Each frame shows seven double-walled nanotubes with diameters in the range of 5–20 nm. Five groups of double-walled nanotubes are presented (from left to right): ZZ@ZZ $(n,0)@(n + 8,0)$; AC@AC $(n,n)@(n + 4,n + 4)$, $(n,n)@(n + 5,n + 5)$ and $(n,n)@(n + 6,n + 6)$; and ZZ@AC. For the ZZ@ZZ systems the $n = 55$, 80, 105, 130, 155, 180, and 243 nanotubes are chosen. For the AC@AC systems the $n = 31$, 46, 60, 75, 89, 104, and 140 are chosen. For the ZZ@AC systems, the following set is considered: (54,0)@(36,36), (80,0)@(51,51), (104,0)@(65,65), (130,0)@(80,80), (154,0)@(94,94), (179,0)@(108,108), and (241,0)@(144,144). The local registry index color bar (right) ranges from blue to red, representing the optimal and worst stacking modes of graphene and *h*-BN, respectively. Grey, pink, and blue spheres on the right-hand-side represent carbon, boron, and nitrogen atoms, respectively. (Reprinted with permission from Leven et al. (2016b). Copyright (2016) by the American Physical Society)

both nanotube walls are of the same type (either zigzag (ZZ) or armchair (AC)), it was found that above a critical diameter that corresponds well with experimental observations (Garel et al. 2012), evenly spaced extended axial facets form (see Fig. 6). Notably, the number of facets equals the interlayer difference in number of circumferential unit-cells. Interestingly, similar axial facets are formed also for mono-chiral double-walled nanotubes, where both nanotube walls are chiral but share the same chiral angle (see left column in Fig. 7). Elongated helical facets, similar to those commonly observed in experiment, appear in nanotubes that exhibit small interlayer chiral angle mismatch (see middle columns in Fig. 7). These are gradually suppressed with increasing interwall chiral angle difference resulting in outer layer corrugation, which is induced by the moiré superlattice, in agreement with experiments (Schouteden et al. 2013). Since multiwalled boron-nitride nanotubes exhibit better interwall chiral angle matching (Celik-Aktas et al. 2005a; Golberg et al. 1999, 2000; Celik-Aktas et al. 2005b) than their carbon counterparts (Schouteden et al. 2013; Zuo et al. 2003; Li et al. 2003; Koziol et al.

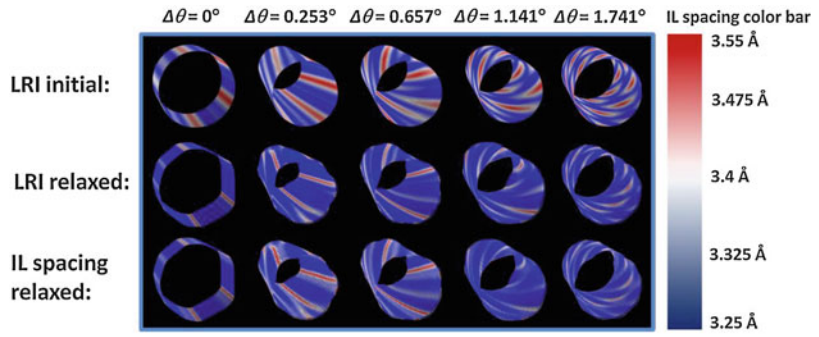

Fig. 7 Schematic representation of (120,100)@(126,105) (leftmost column), (60,60)@(66,65) (second column), (70,70)@(77,74) (third column), (68,68)@(75,70) (fourth column), and (71,71)@(80,72) (rightmost column) double-walled boron-nitride nanotubes showing their local interlayer registry patterns before (top row) and after (middle row) geometry relaxation. The color bar on the right refers to the interlayer spacing of the different systems presented in the bottom row. The colors used in the local registry index patterns are the same as in Fig. 6 above. The chiral angle difference between the inner and outer shells is indicated at the top of each column. (Reprinted with permission from Leven et al. (2016b). Copyright (2016) American Chemical Society)

2005; Hashimoto et al. 2005; Xu et al. 2006; Ducati et al. 2006; Hirahara et al. 2006; Gao et al. 2006; Guo and Guo 2007; Guan et al. 2008), these findings rationalize the experimental observation of relative abundance of faceting in the former (Celik-Aktas et al. 2005a, b; Golberg et al. 1999, 2000).

In resemblance to the effect of moiré structures on the interlayer sliding friction of planar interfaces, nanotube circumferential faceting is expected to have a notable impact on the interwall sliding friction. When the relative axial or angular alignment of adjacent nanotube walls is varied, the corresponding interwall lattice registry changes. If the nanotube is faceted, then this modification results in rearrangement of the faceted superstructure (Guerra et al. 2017). In the case of achiral or mono-chiral double-walled nanotubes, where the facets are axially aligned, a series of unfaceting and refaceting events occurs during the interwall motion accompanied by facet rotation and reconfiguration (see Fig. 8a, b). For bi-chiral systems, where helical facets appear, interwall telescoping results in rotation of the entire faceted superstructure akin to a rotating Archimedean screw (see Fig. 8c). These global structural variations introduce new dissipative channels that enhance interwall friction (Guerra et al. 2017). This, along with the above-mentioned fact that faceting is more abundant in multiwalled boron-nitride nanotubes than in their carbon counterparts, may rationalize recent experimental measurements showing that the former exhibit enhanced interwall friction (Nigues et al. 2014).

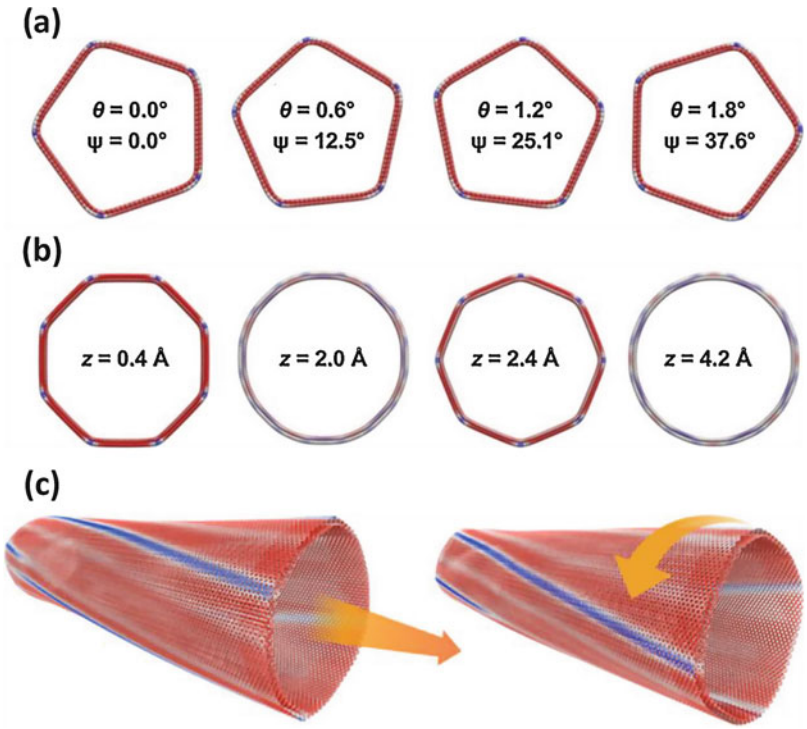

Fig. 8 Facet reconfiguration during interwall pull-out and rotation in (**a**) armchair (104,104)@(109,109); (**b**) zigzag (180,0)@(188,0); and (**c**) bichiral (70,70)@(77,74) double-walled boron-nitride nanotubes. θ, z, and Ψ values appearing in panels (**a**) and (**b**) indicate the relative angular and axial positions of the outer and inner walls and the corresponding facet rotation angle, respectively. The two configurations appearing in panel (**c**) have relative interwall angular and axial orientations of 0.2°/2.4 Å (left) and 0.2°/3.2 Å (right). These correspond to configurations close to the maximum and minimum of the interwall sliding-rotation potential energy surface, respectively. Red, white, and blue atom false coloring indicate low, average, and high atomic interlayer energy, respectively. (Reprinted with permission from Guerra et al. (2017). Copyright (2017) American Chemical Society)

5 Summary

Two-dimensional hexagonal layered materials are of the most promising systems in the field of material science to deliver new technological breakthroughs. The large variety of members in this family and their diverse chemical and physical properties form a vast playground for the design of homogeneous and heterogeneous systems presenting novel structure-function relations. The small dimensions characterizing this field of research call for a synergic interplay between experiment, theory, and computation. With this respect, carefully tailored classical force-field may provide valuable insights on the atomistic nature of different structural, mechanical,

dynamical, and tribological phenomena found in these systems. In the present chapter, a review of recent advances in the field of anisotropic force-fields for describing the interlayer interactions in hexagonal layered materials has been provided. The performance of such force-fields was demonstrated via several applications that address the structural and frictional properties of planar hetero-junctions of graphene and *h*-BN as well as faceted double-walled nanotubes. The good agreement obtained with several experimental observations indicates the predictive power of the developed interlayer force-fields and their ability to rationalize experimental results. The extension of such dedicated force-fields to treat other layered materials is an ongoing effort that, when fulfilled, is expected to enable the discovery of novel low-dimensional structures. Furthermore, the utilization of such force-fields within the framework of multiscale modeling as a source of reliable atomistic information for coarse grained and continuum treatments (Leven et al. 2013; Koren et al. 2016; Leven et al. 2016a; Jung et al. 2015; Kumar et al. 2015; Marom et al. 2010; Hod 2010; Hod 2012b; Blumberg et al. 2012; Garel et al. 2012; Hod 2013; Oz et al. 2016; Leven et al. 2016b; Girifalco 1992; Last et al. 1999; Shenoy et al. 2008; Lu et al. 2009; Yang et al. 2011; Chenxi et al. 2014; Ruiz et al. 2015; Ward 2016; Lebedev et al. 2016) may lead to the development of new nano- and microelectromechanical systems with diverse functionalities based on the promising concepts of 2D layered materials.

Acknowledgments The author is grateful to the Israel Science Foundation for generous financial support under Grant no. 1586/17 and The Naomi Foundation for generous financial support via the 2017 Kadar Award.

References

Al-Jishi R, Dresselhaus G (1982) Lattice-dynamical model for graphite. Phys Rev B 26:4514–4522

Allen MP, Tildesley DJ (2009) Computer simulation of liquids. Oxford University Press, New York

Ambrosetti A, Reilly AM, DiStasio RA, Tkatchenko A (2014) Long-range correlation energy calculated from coupled atomic response functions. J Chem Phys 140:18A508

Argentero G, Mittelberger A, Reza Ahmadpour Monazam M, Cao Y, Pennycook TJ, Mangler C, Kramberger C, Kotakoski J, Geim AK, Meyer JC (2017) Unraveling the 3D atomic structure of a suspended graphene/hBN van der Waals heterostructure. Nano Lett 17:1409–1416

Balandin AA, Ghosh S, Bao W, Calizo I, Teweldebrhan D, Miao F, Lau CN (2008) Superior thermal conductivity of single-layer graphene. Nano Lett 8:902–907

Barone V, Hod O, Peralta JE, Scuseria GE (2011) Accurate prediction of the electronic properties of low-dimensional graphene derivatives using a screened hybrid density functional. Acc Chem Res 44:269–279

Bets KV, Yakobson BI (2009) Spontaneous twist and intrinsic instabilities of pristine graphene nanoribbons. Nano Res 2:161–166

Blumberg A, Keshet U, Zaltsman I, Hod O (2012) Interlayer registry to determine the sliding potential of layered metal dichalcogenides: the case of 2H-MoS2. J Phys Chem Lett 3:1936–1940

Brenner DW (1988) Tersoff-type potentials for carbon, hydrogen and oxygen. Mat Res Soc Symp Proc 141:59–64

Brenner DW (1990) Empirical potential for hydrocarbons for use in simulating the chemical vapor deposition of diamond films. Phys Rev B 42:9458–9471

Brenner DW, Shenderova OA, Harrison JA, Stuart SJ, Ni B, Sinnott SB (2002) A second-generation reactive empirical bond order (REBO) potential energy expression for hydrocarbons. J Phys Condens Matter 14:783

Brunier TM, Drew MGB, Mitchell PCH (1992) Molecular mechanics studies of molybdenum disulphide catalysts parameterisation of molybdenum and sulphur. Mol Sim 9:143–159

Bucholz EW, Sinnott SB (2013) Structural effects on mechanical response of MoS2 nanostructures during compression. J Appl Phys 114:034308

Buldum A, Lu JP (1999) Atomic scale sliding and rolling of carbon nanotubes. Phys Rev Lett 83:5050–5053

Bultinck P, Langenaeker W, Lahorte P, De Proft F, Geerlings P, Waroquier M, Tollenaere JP (2002) The electronegativity equalization method I: parametrization and validation for atomic charge calculations. J Phys Chem A 106:7887–7894

Butz B, Dolle C, Niekiel F, Weber K, Waldmann D, Weber HB, Meyer B, Spiecker E (2014) Dislocations in bilayer graphene. Nature 505:533–537

Cai W, Moore AL, Zhu Y, Li X, Chen S, Shi L, Ruoff RS (2010) Thermal transport in suspended and supported monolayer graphene grown by chemical vapor deposition. Nano Lett 10:1645–1651

Carlson A, Dumitrică T (2007) Extended tight-binding potential for modelling intertube interactions in carbon nanotubes. Nanotechnology 18:065706

Celik-Aktas A, Zuo JM, Stubbins JF, Tang CC, Bando Y (2005a) Double-helix structure in multiwall boron nitride nanotubes. Acta Crystallogr Sect A 61:533–541

Celik-Aktas A, Zuo JM, Stubbins JF, Tang C, Bando Y (2005b) Structure and chirality distribution of multiwalled boron nitride nanotubes. Appl Phys Lett 86:133110

Che J, Çağın T, Deng W, Goddard WA (2000) Thermal conductivity of diamond and related materials from molecular dynamics simulations. J Chem Phys 113:6888–6900

Chen Y, Shen Z, Xu Z, Hu Y, Xu H, Wang S, Guo X, Zhang Y, Peng L, Ding F, Liu Z, Zhang J (2013) Helicity-dependent single-walled carbon nanotube alignment on graphite for helical angle and handedness recognition. Nat Commun 4:2205

Chen Z-G, Shi Z, Yang W, Lu X, Lai Y, Yan H, Wang F, Zhang G, Li Z (2014) Observation of an intrinsic bandgap and Landau level renormalization in graphene/boron-nitride heterostructures. Nat Commun 5:4461

Chenxi Z, Jizhou S, Qingda Y (2014) Periodic buckling patterns of graphene/hexagonal boron nitride heterostructure. Nanotechnology 25:445401

Costamagna S, Neek-Amal M, Los JH, Peeters FM (2012) Thermal rippling behavior of graphane. Phys Rev B 86:041408

Dai S, Ma Q, Liu MK, Andersen T, Fei Z, Goldflam MD, Wagner M, Watanabe K, Taniguchi T, Thiemens M, Keilmann F, Janssen GCAM, Zhu SE, Jarillo Herrero P, Fogler MM, Basov DN (2015) Graphene on hexagonal boron nitride as a tunable hyperbolic metamaterial. Nat Nano 10:682–686

Das S, Robinson JA, Dubey M, Terrones H, Terrones M (2015) Beyond graphene: progress in novel two-dimensional materials and van der Waals solids. Ann Rev Mater Res 45:1–27

David JA, Lincoln DC, Mark TL (2010) Embedded ribbons of graphene allotropes: an extended defect perspective. New J Phys 12:125006

Dean CR, Young AF, Meric I, Lee C, Wang L, Sorgenfrei S, Watanabe K, Taniguchi T, Kim P, Shepard KL, Hone J (2010) Boron nitride substrates for high-quality graphene electronics. Nat Nano 5:722–726

Dean CR, Wang L, Maher P, Forsythe C, Ghahari F, Gao Y, Katoch J, Ishigami M, Moon P, Koshino M, Taniguchi T, Watanabe K, Shepard KL, Hone J, Kim P (2013) Hofstadter's butterfly and the fractal quantum hall effect in moiré superlattices. Nature 497:598–602

Deng D, Novoselov KS, Fu Q, Zheng N, Tian Z, Bao X (2016) Catalysis with two-dimensional materials and their heterostructures. Nat Nano 11:218–230

Dienwiebel M, Verhoeven GS, Pradeep N, Frenken JWM, Heimberg JA, Zandbergen HW (2004) Superlubricity of graphite. Phys Rev Lett 92:126101

Ducati C, Koziol K, Friedrichs S, Yates TJV, Shaffer MS, Midgley PA, Windle AH (2006) Crystallographic order in multi-walled carbon nanotubes synthesized in the presence of nitrogen. Small 2:774–784

Ewald PP (1921) Die Berechnung optischer und elektrostatischer Gitterpotentiale. Ann Phys 369:253–287

Fan Y, Zhao M, Wang Z, Zhang X, Zhang H (2011) Tunable electronic structures of graphene/boron nitride heterobilayers. Appl Phys Lett 98:083103

Fasolino A, Los JH, Katsnelson MI (2007) Intrinsic ripples in graphene. Nat Mater 6:858–861

Frenkel D, Smit B (2002) Understanding molecular simulation. Academic, San Diego

Gao M, Zuo JM, Zhang R, Nagahara LA (2006) Structure determinations of double-wall carbon nanotubes grown by catalytic chemical vapor deposition. J Mater Sci 41:4382–4388

Garel J, Leven I, Zhi C, Nagapriya KS, Popovitz-Biro R, Golberg D, Bando Y, Hod O, Joselevich E (2012) Ultrahigh torsional stiffness and strength of boron nitride nanotubes. Nano Lett 12:6347–6352

Garel J, Zhao C, Popovitz-Biro R, Golberg D, Wang W, Joselevich E (2014) BCN nanotubes as highly sensitive torsional electromechanical transducers. Nano Lett 14:6132–6137

Geim AK (2009) Graphene: status and prospects. Science 324:1530–1534

Geim AK, Grigorieva IV (2013) Van der Waals heterostructures. Nature 499:419–425

Geim AK, Novoselov KS (2007) The rise of graphene. Nat Mater 6:183–191

Ghiringhelli LM, Los JH, Meijer EJ, Fasolino A, Frenkel D (2005a) Modeling the phase diagram of carbon. Phys Rev Lett 94:145701

Ghiringhelli LM, Los JH, Fasolino A, Meijer EJ (2005b) Improved long-range reactive bond-order potential for carbon. II. Molecular simulation of liquid carbon. Phys Rev B 72:214103

Ghiringhelli LM, Valeriani C, Los JH, Meijer EJ, Fasolino A, Frenkel D (2008) State-of-the-art models for the phase diagram of carbon and diamond nucleation. Mol Phys 106:2011–2038

Girifalco LA (1992) Molecular properties of fullerene in the gas and solid phases. J Phys Chem 96:858–861

Girifalco LA, Hodak M (2002) Van der Waals binding energies in graphitic structures. Phys Rev B 65:125404

Girifalco LA, Lad RA (1956) Energy of cohesion, compressibility, and the potential energy functions of the graphite system. J Chem Phys 25:693–697

Girifalco LA, Hodak M, Lee RS (2000) Carbon nanotubes, buckyballs, ropes, and a universal graphitic potential. Phys Rev B 62:13104–13110

Gogotsi Y, Libera JA, Kalashnikov N, Yoshimura M (2000) Graphite polyhedral crystals. Science 290:317–320

Golberg D, Han W, Bando Y, Bourgeois L, Kurashima K, Sato T (1999) Fine structure of boron nitride nanotubes produced from carbon nanotubes by a substitution reaction. J Appl Phys 86:2364–2366

Golberg D, Bando Y, Kurashima K, Sato T (2000) Ropes of BN multi-walled nanotubes. Solid State Commun 116:1–6

Golberg D, Mitome M, Bando Y, Tang CC, Zhi CY (2007a) Multi-walled boron nitride nanotubes composed of diverse cross-section and helix type shells. Appl Phys A Mater Sci 88:347–352

Golberg D, Costa PMFJ, Lourie O, Mitome M, Bai X, Kurashima K, Zhi C, Tang C, Bando Y (2007b) Direct force measurements and kinking under elastic deformation of individual multiwalled boron nitride nanotubes. Nano Lett 7:2146–2151

González Noya E, Srivastava D, Chernozatonskii LA, Menon M (2004) Thermal conductivity of carbon nanotube peapods. Phys Rev B 70:115416

Green JF, Bolland TK, Bolland JW (1974) Lennard-Jones interaction for hexagonal layered crystals. J Chem Phys 61:1637–1646

Guan L, Suenaga K, Iijima S (2008) Smallest carbon nanotube assigned with atomic resolution accuracy. Nano Lett 8:459–462

Guerra R, Tartaglino U, Vanossi A, Tosatti E (2010) Ballistic nanofriction. Nat Mater 9:634–637

Guerra R, Leven I, Vanossi A, Hod O, Tosatti E (2017) Smallest Archimedean screw: facet dynamics and friction in multiwalled nanotubes. Nano Lett 17:5321–5328

Guo W, Guo Y (2007) Energy optimum chiralities of multiwalled carbon nanotubes. J Am Chem Soc 129:2730–2731
Guo Y, Guo W, Chen C (2007) Modifying atomic-scale friction between two graphene sheets: a molecular-force-field study. Phys Rev B 76:155429
Hashimoto A, Suenaga K, Urita K, Shimada T, Sugai T, Bandow S, Shinohara H, Iijima S (2005) Atomic correlation between adjacent graphene layers in double-wall carbon nanotubes. Phys Rev Lett 94:045504
Heine T (2015) Transition metal chalcogenides: ultrathin inorganic materials with tunable electronic properties. Acc Chem Res 48:65–72
Hertel T, Walkup RE, Avouris P (1998) Deformation of carbon nanotubes by surface van der Waals forces. Phys Rev B 58:13870–13873
Heyd J, Scuseria GE (2004a) Assessment and validation of a screened Coulomb hybrid density functional. J Chem Phys 120:7274–7280
Heyd J, Scuseria GE (2004b) Efficient hybrid density functional calculations in solids: assessment of the Heyd–Scuseria–Ernzerhof screened Coulomb hybrid functional. J Chem Phys 121: 1187–1192
Heyd J, Scuseria GE, Ernzerhof M (2003) Hybrid functionals based on a screened Coulomb potential. J Chem Phys 118:8207–8215
Hirahara K, Kociak M, Bandow S, Nakahira T, Itoh K, Saito Y, Iijima S (2006) Chirality correlation in double-wall carbon nanotubes as studied by electron diffraction. Phys Rev B 73:195420
Hod O (2010) Quantifying the stacking registry matching in layered materials. Isr J Chem 50: 506–514
Hod O (2012a) Graphite and hexagonal boron-nitride have the same interlayer distance. Why? J Chem Theory Comput 8:1360–1369
Hod O (2012b) Interlayer commensurability and superlubricity in rigid layered materials. Phys Rev B 86:075444
Hod O (2013) The registry index: a quantitative measure of materials′ interfacial commensurability. ChemPhysChem 14:2376–2391
Hohenberg P, Kohn W (1964) Inhomogeneous electron gas. Phys Rev 136:B864–B871
Jayasena B, Reddy CD, Subbiah S (2013) Separation, folding and shearing of graphene layers during wedge-based mechanical exfoliation. Nanotechnology 24:205301
Jiang J-W (2014a) Registry effect on the thermal conductivity of few-layer graphene. J Appl Phys 116:164313
Jiang JW (2014b) The buckling of single-layer MoS2 under uniaxial compression. Nanotechnology 25:355402
Jiang J-W (2015) Graphene versus MoS2: a short review. Front Phys 10:287–302
Jiang J-W, Park HS (2014) Mechanical properties of MoS2/graphene heterostructures. Appl Phys Lett 105:033108
Jiang J-W, Park HS (2015) A Gaussian treatment for the friction issue of Lennard-Jones potential in layered materials: application to friction between graphene, MoS2, and black phosphorus. J Appl Phys 117:124304
Jiang J-W, Park HS, Rabczuk T (2013) Molecular dynamics simulations of single-layer molybdenum disulphide (MoS2): stillinger-weber parametrization, mechanical properties, and thermal conductivity. J Appl Phys 114:064307
Jiménez Sandoval S, Yang D, Frindt RF, Irwin JC (1991) Raman study and lattice dynamics of single molecular layers of MoS2. Phys Rev B 44:3955–3962
Jin-Wu J, Zenan Q, Harold SP, Timon R (2013) Elastic bending modulus of single-layer molybdenum disulfide (MoS2): finite thickness effect. Nanotechnology 24:435705
Jung J, DaSilva AM, MacDonald AH, Adam S (2015) Origin of band gaps in graphene on hexagonal boron nitride. Nat Commun 6:6308
Kang JW, Lee KW (2014) Molecular dynamics simulation of square graphene-nanoflake oscillator on graphene nanoribbon. J Nanosci Nanotechnol 14:9158–9164
Karssemeijer LJ, Fasolino A (2011) Phonons of graphene and graphitic materials derived from the empirical potential LCBOPII. Surf Sci 605:1611–1615

Kohn W, Sham LJ (1965) Self-consistent equations including exchange and correlation effects. Phys Rev 140:A1133–A1138
Kolmogorov AN, Crespi VH (2000) Smoothest bearings: interlayer sliding in multiwalled carbon nanotubes. Phys Rev Lett 85:4727–4730
Kolmogorov AN, Crespi VH (2005) Registry-dependent interlayer potential for graphitic systems. Phys Rev B 71:235415
Koren E, Lörtscher E, Rawlings C, Knoll AW, Duerig U (2015) Adhesion and friction in mesoscopic graphite contacts. Science 348:679–683
Koren E, Leven I, Lörtscher E, Knoll A, Hod O, Duerig U (2016) Coherent commensurate electronic states at the interface between misoriented graphene layers. Nat Nano 11:752–757
Korhonen T, Koskinen P (2015) Peeling of multilayer graphene creates complex interlayer sliding patterns. Phys Rev B 92:115427
Koziol K, Shaffer M, Windle A (2005) Three-dimensional internal order in multiwalled carbon nanotubes grown by chemical vapor deposition. Adv Mater 17:760–763
Kumar H, Er D, Dong L, Li J, Shenoy VB (2015) Elastic deformations in 2D van der Waals heterostructures and their impact on optoelectronic properties: predictions from a multiscale computational approach. Sci Rep 5:10872
Kushima A, Qian X, Zhao P, Zhang S, Li J (2015) Ripplocations in van der Waals layers. Nano Lett 15:1302–1308
Kuzuba T, Sato T, Ishii T, Arai T (1985) Interlayer binding of hexagonal boron nitride in the rigid-layer approximation. Phys Rev B 32:1230–1236
Kwon Y-K, Tománek D (1998) Electronic and structural properties of multiwall carbon nanotubes. Phys Rev B 58:R16001–R16004
Kwon Y-K, Tománek D (2000) Orientational melting in carbon nanotube ropes. Phys Rev Lett 84:1483–1486
Last JA, Hooks DE, Hillier AC, Ward MD (1999) The physicochemical origins of coincident epitaxy in molecular overlayers: lattice modeling vs potential energy calculations. J Phys Chem B 103:6723–6733
Lebedev AV, Lebedeva IV, Knizhnik AA, Popov AM (2016) Interlayer interaction and related properties of bilayer hexagonal boron nitride: Ab initio study. RSC Adv 6:6423–6435
Lebedeva IV, Knizhnik AA, Popov AM, Ershova OV, Lozovik YE, Potapkin BV (2011a) Diffusion and drift of graphene flake on graphite surface. J Chem Phys 134:104505
Lebedeva IV, Knizhnik AA, Popov AM, Lozovik YE, Potapkin BV (2011b) Interlayer interaction and relative vibrations of bilayer graphene. Phys Chem Chem Phys 13:5687–5695
Lebedeva IV, Knizhnik AA, Popov AM, Lozovik YE, Potapkin BV (2012) Modeling of graphene-based NEMS. Phys E 44:949–954
Lee C, Wei X, Kysar JW, Hone J (2008) Measurement of the elastic properties and intrinsic strength of monolayer graphene. Science 321:385–388
Leven I, Krepel D, Shemesh O, Hod O (2013) Robust superlubricity in graphene/*h*-BN heterojunctions. J Phys Chem Lett 4:115–120
Leven I, Azuri I, Kronik L, Hod O (2014) Inter-layer potential for hexagonal boron nitride. J Chem Phys 140:104106
Leven I, Maaravi T, Azuri I, Kronik L, Hod O (2016a) Interlayer potential for graphene/*h*-BN heterostructures. J Chem Theor Comput 12:2896–2905
Leven I, Guerra R, Vanossi A, Tosatti E, Hod O (2016b) Multiwalled nanotube faceting unravelled. Nat Nano 11:1082–1086
Levendorf MP, Kim C-J, Brown L, Huang PY, Havener RW, Muller DA, Park J (2012) Graphene and boron nitride lateral heterostructures for atomically thin circuitry. Nature 488:627–632
Li D, Kaner RB (2008) Graphene-based materials. Science 320:1170–1171
Li X, Zhu H (2015) Two-dimensional MoS2: properties, preparation, and applications. J Mater 1:33–44
Li F, Chou SG, Ren W, Gardecki JA, Swan AK, Ünlü MS, Goldberg BB, Cheng H-M, Dresselhaus MS (2003) Identification of the constituents of double-walled carbon nanotubes using Raman spectra taken with different laser-excitation energies. J Mater Res 18:1251–1258

Liang T, Phillpot SR, Sinnott SB (2009) Parametrization of a reactive many-body potential for Mo-S systems. Phys Rev B 79:245110
Lindsay L, Broido DA (2010) Optimized Tersoff and Brenner empirical potential parameters for lattice dynamics and phonon thermal transport in carbon nanotubes and graphene. Phys Rev B 81:205441
Lindsay L, Broido DA (2011) Enhanced thermal conductivity and isotope effect in single-layer hexagonal boron nitride. Phys Rev B 84:155421
Liu M, Cowley JM (1994) Structures of the helical carbon nanotubes. Carbon 32:393–403
Liu B, Meng F, Reddy CD, Baimova JA, Srikanth N, Dmitriev SV, Zhou K (2015) Thermal transport in a graphene-MoS2 bilayer heterostructure: a molecular dynamics study. RSC Adv 5:29193–29200
Los JH, Fasolino A (2003) Intrinsic long-range bond-order potential for carbon: performance in Monte Carlo simulations of graphitization. Phys Rev B 68:024107
Los JH, Ghiringhelli LM, Meijer EJ, Fasolino A (2005) Improved long-range reactive bond-order potential for carbon. I. Construction. Phys Rev B 72:214102
Lu JP (1997) Elastic properties of carbon nanotubes and nanoropes. Phys Rev Lett 79:1297–1300
Lu JP, Li XP, Martin RM (1992) Ground state and phase transitions in solid C60. Phys Rev Lett 68:1551–1554
Lu WB, Liu B, Wu J, Xiao J, Hwang KC, Fu SY, Huang Y (2009) Continuum modeling of van der Waals interactions between carbon nanotube walls. Appl Phys Lett 94:101917
Maaravi T, Leven I, Azuri I, Kronik L, Hod O (2017) Interlayer potential for homogeneous graphene and hexagonal boron nitride systems: reparametrization for many-body dispersion effects. J Phys Chem C 121:22826–22835. https://pubs.acs.org/doi/10.1021/acs.nanolett.8b02848
Mandelli D, Leven I, Hod O, Urbakh M (2017) Sliding friction of graphene/hexagonal–boron nitride heterojunctions: a route to robust superlubricity. Sci Rep 7:10851
Marom N, Bernstein J, Garel J, Tkatchenko A, Joselevich E, Kronik L, Hod O (2010) Stacking and registry effects in layered materials: the case of hexagonal boron nitride. Phys Rev Lett 105:046801
Marom N, Tkatchenko A, Rossi M, Gobre VV, Hod O, Scheffler M, Kronik L (2011) Dispersion interactions with density-functional theory: benchmarking semiempirical and interatomic pairwise corrected density functionals. J Chem Theor Comput 7:3944–3951
Michel KH, Verberck B (2011) Phonon dispersions and piezoelectricity in bulk and multilayers of hexagonal boron nitride. Phys Rev B 83:115328
Miró P, Ghorbani-Asl M, Heine T (2013) Spontaneous ripple formation in MoS2 monolayers: electronic structure and transport effects. Adv Mater 25:5473–5475
Mohamed AO, Deepak S (2001) Temperature dependence of the thermal conductivity of single-wall carbon nanotubes. Nanotechnology 12:21
Morita Y, Onodera T, Suzuki A, Sahnoun R, Koyama M, Tsuboi H, Hatakeyama N, Endou A, Takaba H, Kubo M, Del Carpio CA, Shin-yoshi T, Nishino N, Suzuki A, Miyamoto A (2008) Development of a new molecular dynamics method for tribochemical reaction and its application to formation dynamics of MoS2 tribofilm. Appl Surf Sci 254:7618–7621
Morozov SV, Novoselov KS, Katsnelson MI, Schedin F, Elias DC, Jaszczak JA, Geim AK (2008) Giant intrinsic carrier mobilities in graphene and its bilayer. Phys Rev Lett 100:016602
Mortier WJ, Ghosh SK, Shankar S (1986) Electronegativity-equalization method for the calculation of atomic charges in molecules. J Am Chem Soc 108:4315–4320
Neek-Amal M, Peeters FM (2014) Graphene on hexagonal lattice substrate: stress and pseudo-magnetic field. Appl Phys Lett 104:173106
Nicolini P, Polcar T (2016) A comparison of empirical potentials for sliding simulations of MoS2. Comput Mater Sci 115:158–169
Nightingale MP, Umrigar CJ (eds) (1999) Quantum Monte Carlo methods in physics and chemistry. Springer, Netherlands
Nigues A, Siria A, Vincent P, Poncharal P, Bocquet L (2014) Ultrahigh interlayer friction in multiwalled boron nitride nanotubes. Nat Mater 13:688–693

Njo SL, Fan J, van de Graaf B (1998) Extending and simplifying the electronegativity equalization method. J Mol Catal A 134:79–88

Novoselov KS, Geim AK, Morozov SV, Jiang D, Zhang Y, Dubonos SV, Grigorieva IV, Firsov AA (2004) Electric field effect in atomically thin carbon films. Science 306:666–669

Novoselov KS, Geim AK, Morozov SV, Jiang D, Katsnelson MI, Grigorieva IV, Dubonos SV, Firsov AA (2005a) Two-dimensional gas of massless Dirac fermions in graphene. Nature 438:197–200

Novoselov KS, Jiang D, Schedin F, Booth TJ, Khotkevich VV, Morozov SV, Geim AK (2005b) Two-dimensional atomic crystals. Proc Natl Acad Sci U S A 102:10451–10453

Novoselov KS, Mishchenko A, Carvalho A, Castro Neto AH (2016) 2D materials and van der Waals heterostructures. Science 353:aac9439

O'Connor TC, Andzelm J, Robbins MO (2015) AIREBO-M: a reactive model for hydrocarbons at extreme pressures. J Chem Phys 142:024903

Oz I, Leven I, Itkin Y, Buchwalter A, Akulov K, Hod O (2016) Nanotube motion on layered materials: a registry perspective. J Phys Chem C 120:4466–4470

Palser AHR (1999) Interlayer interactions in graphite and carbon nanotubes. Phys Chem Chem Phys 1:4459–4464

Pang T (2016) An introduction to quantum Monte Carlo methods. Morgan & Claypool Publishers, San Rafael

Parr RG, Pearson RG (1983) Absolute hardness: companion parameter to absolute electronegativity. J Am Chem Soc 105:7512–7516

Parr RG, Donnelly RA, Levy M, Palke WE (1978) Electronegativity: the density functional viewpoint. J Chem Phys 68:3801–3807

Perebeinos V, Tersoff J (2009) Valence force model for phonons in graphene and carbon nanotubes. Phys Rev B 79:241409

Ponomarenko LA, Gorbachev RV, Yu GL, Elias DC, Jalil R, Patel AA, Mishchenko A, Mayorov AS, Woods CR, Wallbank JR, Mucha-Kruczynski M, Piot BA, Potemski M, Grigorieva IV, Novoselov KS, Guinea F, Fal'ko VI, Geim AK (2013) Cloning of dirac fermions in graphene superlattices. Nature 497:594–597

Pople JA (1970) Approximate molecular orbital theory (advanced chemistry). McGraw-Hill, New York

Popov AM, Lebedeva IV, Knizhnik AA, Lozovik YE, Potapkin BV (2011) Molecular dynamics simulation of the self-retracting motion of a graphene flake. Phys Rev B 84:245437

Porezag D, Frauenheim T, Köhler T, Seifert G, Kaschner R (1995) Construction of tight-binding-like potentials on the basis of density-functional theory: application to carbon. Phys Rev B 51:12947–12957

Qian D, Liu WK, Ruoff RS (2003) Load transfer mechanism in carbon nanotube ropes. Compos Sci Technol 63:1561–1569

Rao CNR, Sood AK, Subrahmanyam KS, Govindaraj A (2009) Graphene: the new two-dimensional nanomaterial. Angew Chem Int Ed (English) 48:7752–7777

Rapaport DC (2009) The art of molecular dynamics simulation. Cambridge University Press, New York

Rappe AK, Casewit CJ, Colwell KS, Goddard WA, Skiff WM (1992) UFF, a full periodic table force field for molecular mechanics and molecular dynamics simulations. J Amer Chem Soc 114:10024–10035

Reguzzoni M, Fasolino A, Molinari E, Righi MC (2012a) Friction by shear deformations in multilayer graphene. J Phys Chem C 116:21104–21108

Reguzzoni M, Fasolino A, Molinari E, Righi MC (2012b) Potential energy surface for graphene on graphene: Ab initio derivation, analytical description, and microscopic interpretation. Phys Rev B 86:245434

Ruiz L, Xia W, Meng Z, Keten S (2015) A coarse-grained model for the mechanical behavior of multi-layer graphene. Carbon 82:103–115

Sakai Y, Saito S, Cohen ML (2015) First-principles study on graphene/hexagonal boron nitride heterostructures. J Phys Soc Jap 84:121002

Sanderson RT (1951) An interpretation of bond lengths and a classification of bonds. Science 114:670–672
Sanderson RT (1976) Chemical bonds and bond energy, 2nd edn. Academic, New York
Sanderson RT (1983) Polar covalence. Academic, New York
Schouteden K, Volodin A, Li Z, Van Haesendonck C (2013) Atomically resolved moiré-type superstructures in double-walled carbon nanotubes. Carbon 61:379–385
Sevik C, Kinaci A, Haskins JB, Çağın T (2011) Characterization of thermal transport in low-dimensional boron nitride nanostructures. Phys Rev B 84:085409
Shenoy VB, Reddy CD, Ramasubramaniam A, Zhang YW (2008) Edge-stress-induced warping of graphene sheets and nanoribbons. Phys Rev Lett 101:245501
Shibuta Y, Elliott JA (2011) Interaction between two graphene sheets with a turbostratic orientational relationship. Chem Phys Lett 512:146–150
Shtogun YV, Woods LM (2010) Many-body van der Waals interactions between graphitic nanostructures. J Phys Chem Lett 1:1356–1362
Singh SK, Neek-Amal M, Costamagna S, Peeters FM (2013) Thermomechanical properties of a single hexagonal boron nitride sheet. Phys Rev B 87:184106
Singh SK, Neek-Amal M, Costamagna S, Peeters FM (2015) Rippling, buckling, and melting of single- and multilayer MoS2. Phys Rev B 91:014101
Strutyński K, Gomes JANF, Melle-Franco M (2014) Accuracy of dispersion interactions in semiempirical and molecular mechanics models: the benzene dimer case. J Phys Chem A 118:9561–9567
Stuart SJ, Tutein AB, Harrison JA (2000) A reactive potential for hydrocarbons with intermolecular interactions. J Chem Phys 112:6472–6486
Szabados Á, Biró LP, Surján PR (2006) Intertube interactions in carbon nanotube bundles. Phys Rev B 73:195404
Szabo A, Ostlund NS (1989) Modern quantum chemistry: introduction to advanced electronic structure theory. Dover Publications, Mineola
Tang S, Wang H, Zhang Y, Li A, Xie H, Liu X, Liu L, Li T, Huang F, Xie X, Jiang M (2013) Precisely aligned graphene grown on hexagonal boron nitride by catalyst free chemical vapor deposition. Sci Rep 3:2666
Tersoff J (1988) Empirical interatomic potential for carbon, with applications to amorphous carbon. Phys Rev Lett 61:2879–2882
Tersoff J (1992) Energies of fullerenes. Phys Rev B 46:15546–15549
Tersoff J, Ruoff RS (1994) Structural properties of a carbon-nanotube crystal. Phys Rev Lett 73:676–679
Tkatchenko A, Scheffler M (2009) Accurate molecular van der Waals interactions from ground-state electron density and free-atom reference data. Phys Rev Lett 102:073005
Tkatchenko A, DiStasio RA, Car R, Scheffler M (2012) Accurate and efficient method for many-body van der Waals interactions. Phys Rev Lett 108:236402
Tolga A, Jeremy KM, Hakan E (2016) A new interlayer potential for hexagonal boron nitride. J Phys Condens Matter 28:385401
Toukmaji AY, Board JA (1996) Ewald summation techniques in perspective: a survey. Comp Phys Comm 95:73–92
van Duin ACT, Dasgupta S, Lorant F, Goddard WA (2001) Reax FF: a reactive force field for hydrocarbons. J Phys Chem A 105:9396–9409
van Wijk MM, Dienwiebel M, Frenken JWM, Fasolino A (2013) Superlubric to stick-slip sliding of incommensurate graphene flakes on graphite. Phys Rev B 88:235423
van Wijk MM, Schuring A, Katsnelson MI, Fasolino A (2014) Moiré patterns as a probe of interplanar interactions for graphene on *h*-BN. Phys Rev Lett 113:135504
van Wijk MM, Schuring A, Katsnelson MI, Fasolino A (2015) Relaxation of moiré patterns for slightly misaligned identical lattices: graphene on graphite. 2D Mater 2:034010
Vanossi A, Manini N, Urbakh M, Zapperi S, Tosatti E (2013) Colloquium: modeling friction: from nanoscale to mesoscale. Rev Mod Phys 85:529–552

Varshney V, Patnaik SS, Muratore C, Roy AK, Voevodin AA, Farmer BLMD (2010) Simulations of molybdenum disulphide (MoS2): force-field parameterization and thermal transport behavior. Comput Mater Sci 48:101–108

Wakabayashi N, Smith HG, Nicklow RM (1975) Lattice dynamics of hexagonal MoS2 studied by neutron scattering. Phys Rev B 12:659–663

Wang H, Liu F, Fu W, Fang Z, Zhou W, Liu Z (2014) Two-dimensional heterostructures: fabrication, characterization, and application. Nanoscale 6:12250–12272

Ward MD (2016) Soft crystals in flatland: unraveling epitaxial growth. ACS Nano 10:6424–6428

Weismiller MR, Duin ACT v, Lee J, Yetter RA (2010) Reax FF reactive force field development and applications for molecular dynamics simulations of ammonia borane dehydrogenation and combustion. J Phys Chem A 114:5485–5492

Weiss K, Phillips JM (1976) Calculated specific surface energy of molybdenite (MoS2). Phys Rev B 14:5392–5395

Woods CR, Britnell L, Eckmann A, Ma RS, Lu JC, Guo HM, Lin X, Yu GL, Cao Y, Gorbachev RV, Kretinin AV, Park J, Ponomarenko LA, Katsnelson MI, Gornostyrev YN, Watanabe K, Taniguchi T, Casiraghi C, Gao HJ, Geim AK, Novoselov KS (2014) Commensurate-incommensurate transition in graphene on hexagonal boron nitride. Nat Phys 10:451–456

Woods CR, Withers F, Zhu MJ, Cao Y, Yu G, Kozikov A, Ben Shalom M, Morozov SV, van Wijk MM, Fasolino A, Katsnelson MI, Watanabe K, Taniguchi T, Geim AK, Mishchenko A, Novoselov KS (2016) Macroscopic self-reorientation of interacting two-dimensional crystals. Nat Commun 7:10800

Xiaonan W, Alireza T, Douglas ES (2015) Fracture mechanics of monolayer molybdenum disulfide. Nanotechnology 26:175703

Xu Z, Bai X, Wang ZL, Wang E (2006) Multiwall carbon nanotubes made of monochirality graphite shells. J Am Chem Soc 128:1052–1053

Xu Z, Li X, Yakobson BI, Ding F (2013) Interaction between graphene layers and the mechanisms of graphite's superlubricity and self-retraction. Nanoscale 5:6736–6741

Xu X, Pereira LFC, Wang Y, Wu J, Zhang K, Zhao X, Bae S, Tinh Bui C, Xie R, Thong JTL, Hong BH, Loh KP, Donadio D, Li B, Özyilmaz B (2014) Length-dependent thermal conductivity in suspended single-layer graphene. Nat Commun 5:3689

Yang B, Barsoum MW, Rethinam RM (2011) Nanoscale continuum calculation of basal dislocation core structures in graphite. Philoso Mag 91:1441–1463

Yang W, Chen G, Shi Z, Liu C-C, Zhang L, Xie G, Cheng M, Wang D, Yang R, Shi D, Watanabe K, Taniguchi T, Yao Y, Zhang Y, Zhang G (2013) Epitaxial growth of single-domain graphene on hexagonal boron nitride. Nat Mater 12:792–797

Yankowitz M, Xue J, Cormode D, Sanchez-Yamagishi JD, Watanabe K, Taniguchi T, Jarillo-Herrero P, Jacquod P, LeRoy BJ (2012) Emergence of superlattice dirac points in graphene on hexagonal boron nitride. Nat Phys 8:382–386

Yao Z, Wang J-S, Li B, Liu G-R (2005) Thermal conduction of carbon nanotubes using molecular dynamics. Phys Rev B 71:085417

Ye Z, Tang C, Dong Y, Martini A (2012) Role of wrinkle height in friction variation with number of graphene layers. J Appl Phys 112:116102

Ye Z, Otero-de-la-Roza A, Johnson ER, Martini A (2015) Oscillatory motion in layered materials: graphene, boron nitride, and molybdenum disulfide. Nanotechnology 26:165701

Zahid F, Liu L, Zhu Y, Wang J, Guo H (2013) A generic tight-binding model for monolayer, bilayer and bulk MoS2. AIP Adv 3:052111

Ze L (2014) The diversity of friction behavior between bi-layer graphenes. Nanotechnology 25:075703

Zhang G, Jiang X, Wang E (2003) Tubular graphite cones. Science 300:472–474

Zhang GY, Bai XD, Wang EG, Guo Y, Guo W (2005) Monochiral tubular graphite cones formed by radial layer-by-layer growth. Phys Rev B 71:113411

Zuo JM, Vartanyants I, Gao M, Zhang R, Nagahara LA (2003) Atomic resolution imaging of a carbon nanotube from diffraction intensities. Science 300:1419–1421